# Dependence on temperature and salinity gradients and the injection rate of CO2 storage in saline aquifers with an angular unconformity

Pourmalek, A. & Shariatipour, S. M.



**Original citation & hyperlink:**
Pourmalek, A & Shariatipour, SM 2019, 'Dependence on temperature and salinity gradients and the injection rate of CO2 storage in saline aquifers with an angular unconformity' Journal of Porous Media, vol. 22, no. 8, pp. 1065-1078. https://dx.doi.org/10.1615/JPorMedia.2019025077

DOI 10.1615/JPorMedia.2019025077
ISSN 1091-028X
ESSN 1934-0508

Publisher: Begell House

# Dependence on temperature and salinity gradients and the injection rate of $CO_2$ storage in saline aquifers with an angular unconformity

Azadeh Pourmalek* S.M Shariatipour

Centre for Flow Measurement and Fluid Mechanics, Coventry University, UK

*Correspondence: pourmala@uni.coventry.ac.uk

## Abstract

An unconformity surface is a type of interface between an aquifer and a caprock. It refers to a buried erosional or non-depositional surface that separates two strata of different ages, indicating that sediment deposition has not been continuous. A high or low-permeability layer may exist just above or below the unconformity surface. The high-permeability layer could be the result of the weathering and erosion of the older layer, or the deposition of coarse-grained sediments on top of the unconformity surface. The effect of this interface on $CO_2$ dissolution in brine was investigated by running a range of 2D models and considering different injection scenarios. By examining different injection scenarios using two models for comparative analysis (one with and one without a high-permeability layer), the results provide a good hypothesis of the effects of pressure and migration distance on $CO_2$ dissolution. Although the high-permeable layer creates a pathway for the further migration of $CO_2$, the models without a high-permeable layer have tended to predict a higher $CO_2$ dissolution in almost all the injection scenarios. In addition, the sensitivity of $CO_2$ dissolution to aquifer parameters was examined, such as temperature and salinity gradients. Models with and without temperature and salinity gradients were compared and the importance of these parameters on the prediction of $CO_2$ storage was determined. Another significant result is that under higher injection scenarios, the models show significant sensitivity to temperature and salinity gradients. However, for lower

injection rates the sensitivity of the dissolved $CO_2$ to temperature and salinity gradients is almost negligible.

**Keywords:** $CO_2$ storage. Deep saline aquifer. Unconformity. Temperature gradient. Salinity gradient

---

## 1. Introduction

New and robust scientific evidence has provided a solid causal link between anthropogenic activity and global warming over the past 50 years. The composition of the atmosphere is expected to continue changing throughout the 21st century. This is now referred to as the anthrosphere (IPCC 2005; Stern 2006).

Carbon capture and storage (CCS) is one of the measures that can considerably reduce $CO_2$ emissions into the atmosphere. Three possible $CO_2$ storage location types are abandoned oil and gas reservoirs, deep un-mineable coal beds and deep saline aquifers. The main points to consider each of these sites are their suitability for permanent $CO_2$ containment and the extent to which the injected $CO_2$ could leak into the atmosphere or groundwater (Bachu et al. 1993). The most suitable and globally available short-term option for $CO_2$ storage is deep saline aquifers (Bachu et al. 1993). The global $CO_2$ storage capacity of these geological formations is estimated to range from 400 to 10,000 Gt $CO_2$ (Davison et al. 2001). Their storage capacities make them a significant option and an ideal candidate to be deployed as part of a mitigation policy to reduce the $CO_2$ burden (Nordbotten et al. 2005).

Reservoirs are complex systems and deep formations undergo different tectono-sedimentary evolution through geological years (Song et al. 2014). There is a number of different potential trapping mechanisms exist to store $CO_2$ in geological media. $CO_2$ has a lower density compared to the brine in an aquifer and is a buoyant fluid. Therefore, following its injection into a saline

aquifer, the $CO_2$ will move upward under buoyancy to reach a barrier where its migration is prevented by fine-grained rocks (mainly shale) and evaporates, with small pore throat radii in comparison with a reservoir. The $CO_2$ will then spread out underneath the barrier and move laterally, depending on the caprock and aquifer interface. Consequently, the injected $CO_2$ is retained primarily at the top surface interval (Nilsen et al. 2012). Therefore, prior to considering a site for $CO_2$ storage, evaluating the properties of an aquifer and its caprock interface is crucial and has been previously investigated by Shariatipour et al. (2014; 2016a), Nilsen et al. (2012) and Goater et al. (2013).

The morphology between the aquifer and the caprock is determined by sedimentological setting and structural deformation. It has a significant effect on the migration paths and the storage of $CO_2$ (Shariatipour et al. 2016b). An unconformity surface is a type of interface between the aquifer and caprock which refers to a buried erosional or non-depositional surface separating two strata of different ages. Different authors have proposed several trap classifications. However, there is general agreement on three broad categories of trap which are stratigraphic, structural or a combination of both (Biddle, Wielchowsky 1994). Stratigraphic traps are often formed by stratigraphical processes at the time of sediment deposition (Biddle & Wielchowsky 1994). Unconformities are a type of stratigraphic trap and play a crucial role in trapping oil and gas. Therefore, they can similarly provide a stratigraphical trap for storing $CO_2$ as a mitigation action. Categories of unconformity include angular unconformity, disconformity, paraconformity and non-conformity.

An angular unconformity is the most common and most recognisable among unconformities. After a period of deformation of older sediments, tilted layers have been subjected to erosion. Subsequently, a younger sediment has been deposited on top. Just above or just below the unconformity surface, there could be a high-permeability or low-permeability layer. The high-permeability layer could be the result of the weathering and erosion of the older layer of the

unconformity surface or the deposition of coarse-grained sediments on top of the unconformity surface (Swierczek 2012). Shariatipour et al. (2016b) investigated the effects of the unconformity surface on the storage capacity and security of $CO_2$. They showed that an unconformity model with a high-permeability layer at the caprock and aquifer interface can contribute to pressure diffusion through the reservoir.

In their research, Cao et al. (2005) concluded that in the Permian petroleum system (in the north-west margin of the Junggar Basin, China), hydrocarbons migrate vertically alongside faults and laterally alongside the unconformity surface. In addition, several unconformity surfaces exist in the Sikeshu sag of the Junggar basin. Among them, the unconformity surface at the bottom of the Palaeogene is one of the main migration pathways. It suggests that the unconformity surface can act as an efficient medium for fluid transportation (Gao et al. 2013). Fengjun et al. (2001) investigated the sedimentological characteristics of the Zhuhai and Zhujiang Formations (again in China) and specified that sandstone with good porosity and permeability deposited on the unconformity surface acts as the main migration conduit and provides lateral connectivity for generated oils. Studies of Belfast Bay in the western Gulf of Ontario by Rogers et al. (2006) showed that as a conductive layer, the coarse-grained unconformity between Pleistocene glacial-marine mud and Holocene mud may permit gas to migrate towards the field's margins. Therefore, fluid migration can be restricted across the unconformity surface or just into particular areas, but unrestricted fluid migration can also be permitted across the surface. Both conditions depend on the properties of the unconformity surface and therefore on the process involved in creating the unconformities initially. In this research, the effects of the existence or non-existence of this high-permeability layer on $CO_2$ dissolution is investigated, considering different reservoir parameters including temperature, salinity and injection rate.

The supercritical $CO_2$ flow and storage in deep saline aquifers is a complex, two-phase flow in porous media (Song et al. 2015). As mentioned above, $CO_2$ can be sequestered in deep saline aquifers. $CO_2$ and brine are miscible fluids and subsequently, the $CO_2$ dissolves in brine. The composition and concentration level of dissolved salt in brine differs around the world. Sodium chloride is the main dissolved solid in the saline aquifers. Freshwater typically has less than 1000 mg/L total dissolved salt (TDS), dense brine has more than 100,000 mg/L TDS and sea water has about 35,000 mg/L TDS (Oldenburg 2007). Normally, the formation salinity in sedimentary basins gradually increases with depth, with this increase generally being linear, over thousands of metres vertically. The rate of increase ranges from 50 to 300 mg/L/m (Dickey 1969).

The equilibrium temperature of the rock and brine that make up the aquifer also changes linearly with depth. The temperature of the subsurface formation depends on a geothermal gradient in that specific region. The degree of temperature increase with depth can be low in a tectonic subduction zone (where tectonic plates meet), to very high along island arcs and volcanic areas (Peacock 1996; Saemundsson et al. 2009). Furthermore, the geothermal gradient can differ noticeably across a region. For instance, in the North Sea, the gradient varies from 18°C/km south of Norway to more than 40°C/km in the Central Graben off the Danish coast, with an average of 29°C/km (Harper 1971; Evans 1974). In a sedimentary basin, the temperature gradient varies from 10°C/km to 50°C/km (Koide et al. 1995) and according to Holloway (2008); the typical gradient is between 25-30°C/km.

The consequence of the increased temperature is that the density and viscosity of the formation water decrease significantly. As the pressure in the aquifer increases with depth, the density and viscosity increases even with a consequent increase in temperature, but by a less significant amount. The largest increase in density and viscosity is generally observed by an increase in the amount of dissolved solids (TDS) (Bachu and Adam 2003). The pressure, temperature and

salinity of aquifers have significant effects on the ultimate $CO_2$ solubility in the water phase and the aquifer's storage capacity (Bachu and Adams 2003). The solubility of $CO_2$ in water increases with pressure (Spycher et al. 2003; Spycher and Pruess (2005; 2010)) and decreases with temperature and water salinity increase (IPCC 2005). Nordbotten et al. (2005) classified different basins with regard to the degree of geothermal gradient and surface temperature. These are categorised as cold basins (a geothermal gradient of 25°C and a surface temperature of 10°C) and warm basins (a geothermal gradient of 45°C and a surface temperature of 20°C), respectively.

In most cases, the vertical variations in salinity and temperature are ignored in $CO_2$ simulations. Therefore, the original vertical profile of salinity and temperature remains almost unchanged during the simulation period (Shariatipour et al. 2016b). In other words, in previous simulation studies, constant reservoir salinity and temperature were considered. However, as mentioned above, normally formation salinity and temperature in sedimentary basins gradually increase with depth. Therefore, it is necessary to consider temperature and salinity gradient in $CO_2$ storage modelling. In this research, the modelling exercise undertakes the comparative effect of constant reservoir salinity and temperature against variation in these parameters, to assess the relative effect on $CO_2$ dissolution and migration in saline aquifers with unconformity.

## 2. Model description

Numerical simulation is progressively applied for forecasting fluid flow in the porous media (Mousavi Nezhad et al. 2011). Although Numerical simulation software have inadequacies such as long computing time (Song et al. 2014), they are crucial for modeling the $CO_2$ flow in the porous media for CCS technology. A reliable and precise model must completely reflect all the mechanisms involved in the system (Mousavi Nezhad et al. 2011). Fluid flow is significantly affected by the properties of the domain through which the process happens (Mousavi Nezhad et al. 2011). The base model used to investigate the effects of salinity and

147 temperature gradients and the effects of an unconformity surface on $CO_2$ dissolution was an
148 angular unconformity 2D Model with a length of 10 Km, a thickness of 400 m and a width of
149 100 m, which was discretized into 100× 445 ×1 cells. The aquifers were assumed to be
150 homogeneous and the model boundaries assumed to be closed. One injection well was located
151 on the left-hand side of the modelled aquifer. The maximum bottom hole pressure was limited

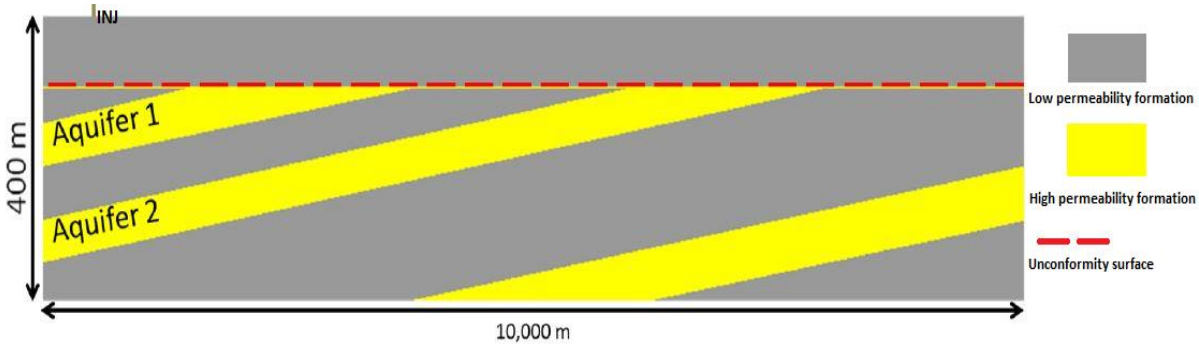


152 Fig. 1 Angular Unconformity (2D) model as a base case (Shariatipour et al. 2016b).

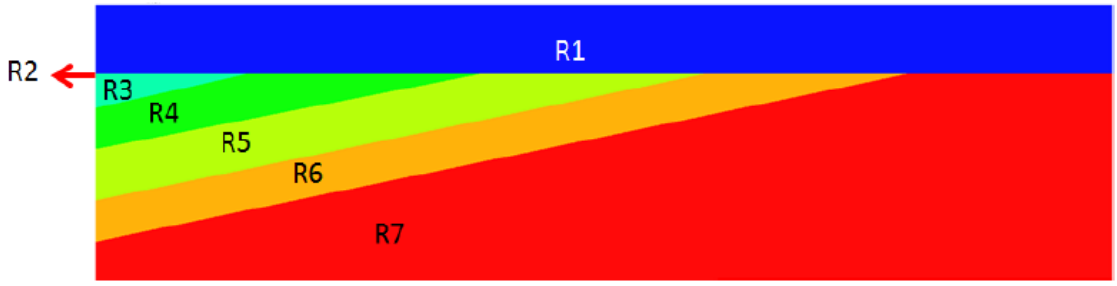


Fig. 2 Seven regions of the model: (R1)-caprock, (R2)-interface between caprock and aquifer (unconformity surface), (R3)-low- permeability layer above aquifer 1, (R4) aquifer 1, (R5)-low- permeability layer between aquifer 1 and 2, (R6)- aquifer2, (R7)-low-permeability layer below aquifer2. R refers to regions (Shariatipour et al. 2016b).

153 to 229 bars. To investigate the effect of an unconformity surface, different injection rate
154 scenarios were taken into consideration as the pressure did not reach the restrictive bottom-
155 hole pressure. The injector was closed after 50 years and the simulation was continued for a
156 further 200 years. The base model is shown in Figure 1 and was taken from Shariatipour et al.
157 (2016b). All models were constructed using Schlumberger's Petrel Modelling© software, and
158 the reservoir models were input into the Schlumberger ECLIPSE© compositional reservoir
159 simulator with the CO2STORE option. The model was divided into seven regions (shown in
160 Figure 2) with the porosity and permeability of each region and model properties shown in

table 1 and 2, respectively. The relative permeability curves used in this model (Smith et al. 2012) is shown in Figure 3.

Table 1 Properties of each region.

| **Formation** | **Porosity** | **Permeability (mD)** |
|---|---|---|
| Caprock (R1) | 10% | 1E-06 |
| Unconformity interface (R2) | 25% | 1000 |
| Low permeable layer above aquifer 1(R3) | 10% | 1E-06 |
| Aquifer 1(R4) | 25% | 1000 |
| Low permeable layer between aquifer 1 and 2 (R5) | 10% | 1E-06 |
| Aquifer 2 (R6) | 25% | 1000 |
| Low permeable layer below aquifer 2 (R7) | 10% | 1E-06 |

Table 2 Model properties.

| **Model parameters** | Value |
|---|---|
| Rock Compressibility ($bar^{-1}$) | $5 \times 10^{-5}$ |
| Fluid Compressibility ($bar^{-1}$) | $3 \times 10^{-5}$ |
| Initial mole fraction | $CO_2$ $H_2O$ NaCl<br>0.0 0.967 0.033 |
| Datum depth (m) | 900 |
| Pressure at datum depth (bar) | 90 |
| Maximum relative permeability to $CO_2$ | 0.0654 |

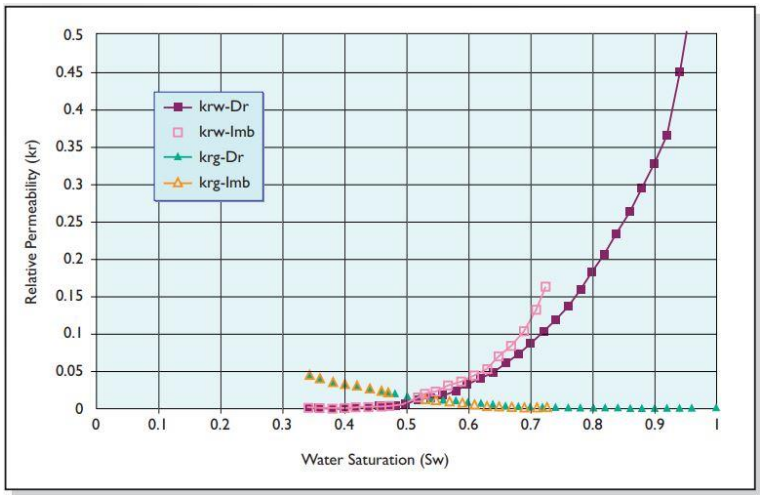


Fig. 3 The relative permeability curves (Smith et al. 2012).

## 3. Effect of a high-permeability layer on $CO_2$ dissolution

Model 1 had a high-permeability layer at the unconformity surface with permeability of the saline aquifers (1000 mD). In this model, $CO_2$ was injected at the bottom of Aquifer 1. Model 2, as with model 1, had a high-permeability layer but $CO_2$ was injected through a perforation at the bottom of Aquifer 2. Models 3 and 4 did not have the high-permeability layer and the unconformity surface had permeability equal to the caprock. The only difference between these two models was the location of the perforation. In Model 3, $CO_2$ was injected at the bottom of Aquifer 1 but in Model 4, $CO_2$ was injected at the bottom of Aquifer 2. Different injection scenarios ($3\times10^3$, $4\times10^3$, $5\times10^3$, $7\times10^3$, $20\times10^3$, $35\times10^3$, $50\times10^3$and $70\times10^3$ $SM^3$ /day) were taken into consideration to investigate the effects of the properties of the interface between the caprock and the aquifer; and therefore, the distance migrated and the pressure on $CO_2$ dissolution. To do so, these eight different injection scenarios were set for each model. This meant that at the end, 32 models were constructed.

Given that the distance from the perforation at the bottom to the caprock of Aquifer 1 was less than that of Aquifer 2, it was therefore predictable that $CO_2$ injected into Aquifer 1 would reach the top much sooner. Moreover, in Models 1 and 2, $CO_2$ could migrate laterally through the permeable layer, as it plays a role as a conductive layer which connects the two aquifers. Therefore, the injected $CO_2$ could reach the second storage formation. In Models 3 and 4, when the high-permeable conductive layer does not exist, the $CO_2$ lateral migration was restricted and the injected $CO_2$ could not reach the second storage formation. Therefore, the properties of the caprock and aquifer interface play an important role as they provide a pathway for $CO_2$ to migrate laterally or to restrict its pathway.

Figure 4 compares the dissolved $CO_2$ in all four models when the injection rate was relatively low ($5\times10^3$ $SM^3$/day). $CO_2$ dissolution in Models 2 and 4 was higher than for Models 1 and 3

(40%). $CO_2$, which is less dense than brine, migrates upward until it reaches the top seal. The distance that the $CO_2$ migrates in Aquifer 2 was far more than in Aquifer 1 and therefore it was in contact with the brine for longer. The dissolution trapping mechanism then plays a far more active role. Regarding the dissolved $CO_2$ in the models with the high-permeable conductive layer (Models 1 and 2) and the models with the low-permeable layer (Models 3 and 4), the $CO_2$ dissolution results using Model 1 were higher than for Model 3, while Model 2 were higher than Model 4 (6%). This is due to the fact that the $CO_2$ migrates laterally through the high-permeable layer and starts to use another aquifer as a second storage formation. In other words, these two aquifers are connected by the high-permeable layer. The obvious difference starts at the 50 years post-injection period as is clear from the figure. During the injection period (50 years), there is no noticeable difference existing between the models with a high-permeable layer and those with a low-permeable layer, since during this period, the $CO_2$ has not reached the conductive layer.

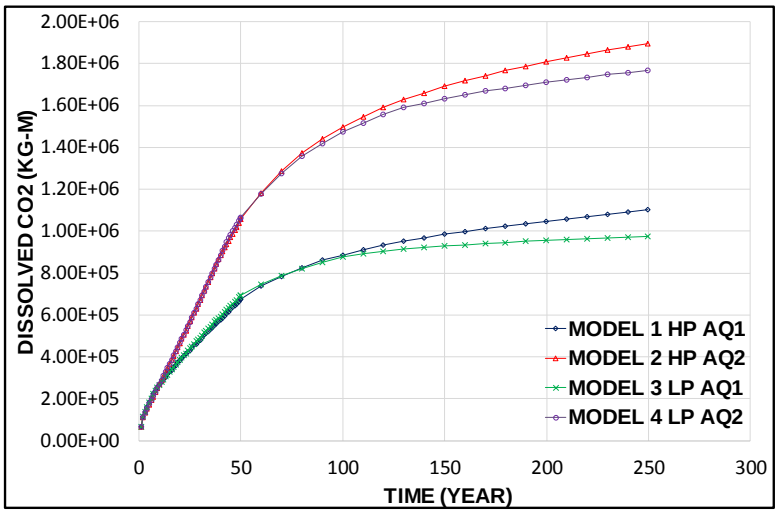


Fig.4 Dissolved $CO_2$ in relatively low injection rate ($5\times10^3$ $SM^3$/day). HP refers to high-permeability and LH refers to Low-permeability.

Figure 5 compares the dissolved $CO_2$ for the four models when the injection rate is relatively high ($70\times10^3$ $SM^3$/day). Most noticeable in this figure is that more $CO_2$ is dissolved in Models 3 and 4 with a low-permeable layer and that the difference is apparent from the middle of the

injection period. This is due to the fact that for higher injection rates, the pressure increases and more $CO_2$ dissolution in brine is triggered by that increase. At the end of the post-injection period, the highest $CO_2$ dissolution is seen in the results of Model 4 with a low-permeable layer at the unconformity surface when the $CO_2$ was injected into Aquifer 2. This is because on the one hand, the $CO_2$ migrates further in Aquifer 2 until it reaches the caprock so there is time for more brine and $CO_2$ interaction. On the other hand, the formation pressure is higher in the closed aquifer when the unconformity interface becomes part of the caprock and no conductive layer exists. The difference observed between the model's results with the $CO_2$ injection at the bottom of Aquifer 1 or Aquifer 2 is not significant. Therefore, in the presence of a low-permeability layer, as long as the pressure does not reach the pressure constraint, the higher injection rate plays a more effective role in $CO_2$ dissolution. The least dissolution had occurred using Model 1. Therefore, more $CO_2$ dissolution occurs in the closed model with a greater distance to the caprock.

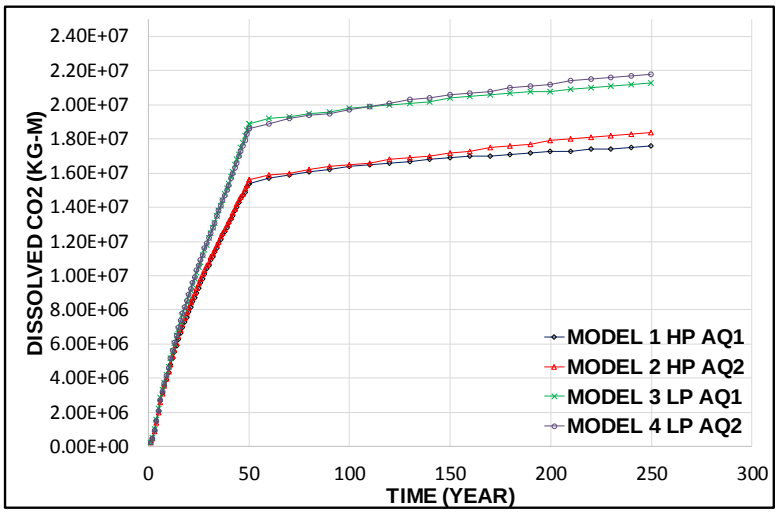


Fig.5 Dissolved $CO_2$ in relatively high injection rate ($70\times10^3$ $SM^3$/day). HP refers to high-permeability and LH refers to low-permeability.

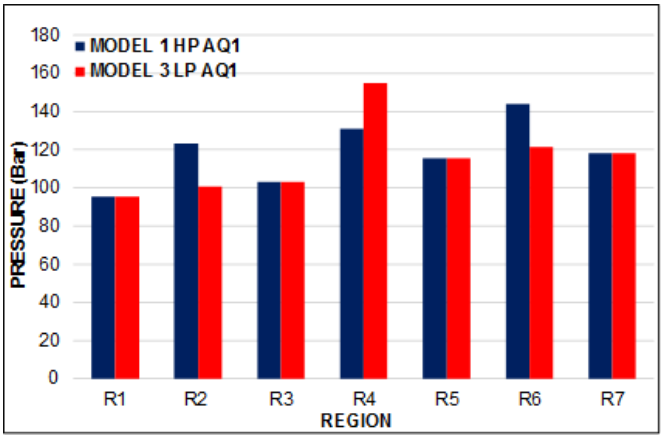


Fig.6 Average pressure when $CO_2$ is injected at the bottom of Aquifer 1 (R as region).

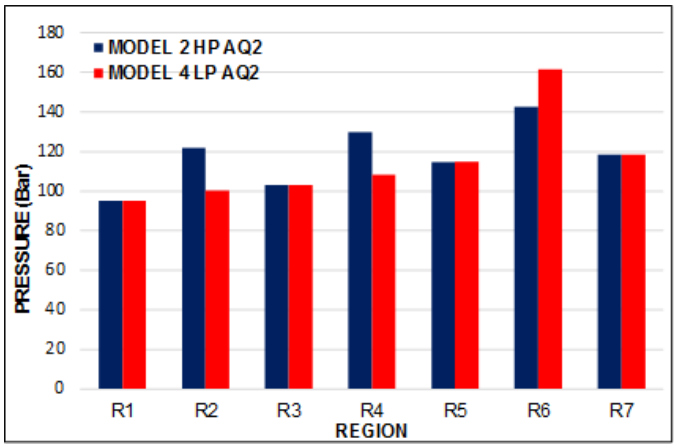


Fig.7 Average pressure when $CO_2$ is injected at the bottom of Aquifer 2 (R as region).

In both figures (6 & 7 above), no significant difference is observable in pressure in the low-permeable regions even after injecting $CO_2$. This is because free $CO_2$ does not enter these regions to increase the pressure. In Figure 6, the highest pressure is experienced in Aquifer 1 (region 4) of Model 3. This is because $CO_2$ was directly injected into this aquifer and also, as for the closed model, the conductive layer does not exist for $CO_2$ migration and pressure diffusion. The average pressure in Aquifer 2 (region 6) of Model 3 does not change since the lateral connectivity is restricted. Therefore, free $CO_2$ cannot migrate laterally to fill Aquifer 2 and increase the pressure. Hence in Model 3, the average pressure in Aquifer 2 is lower than Aquifer 1. However, the pressure in Aquifer 2 (region 6) of Model 1 is increased, since $CO_2$

enters this aquifer through the high-permeability layer. The high-permeability layer contributes to the pressure diffusion from Aquifer 1 to Aquifer 2 (Shariatipour et al. 2016b).

In Figure 7, the average pressure is shown when $CO_2$ is injected into Aquifer 2. As expected, the highest average pressure is observable in Aquifer 2 for the simulations using Model 4 for the reasons explained above.

Figure 8 shows the amount of dissolved $CO_2$ predicted by all the models at the end of the post-injection period. For the lowest injection rate ($3\times10^3$ $SM^3$/day), the lowest amount of dissolved $CO_2$ is observed in Model 3 (7.37E+05 Kg-M). The highest dissolution occurs using Model 2 (1.46E+06 Kg-M), again due to the longer migration distance and therefore, the higher $CO_2$ and brine interaction time. For the highest injection rate studied ($70\times10^3$ $SM^3$/day), the lowest amount of $CO_2$ dissolution occurs using Model 1 (1.73E+07 Kg-M). The highest $CO_2$ dissolution occurs with Model 4 (2.12E+07 Kg-M) because of the combined effects of the greater pressure increase and the longer migration distance.

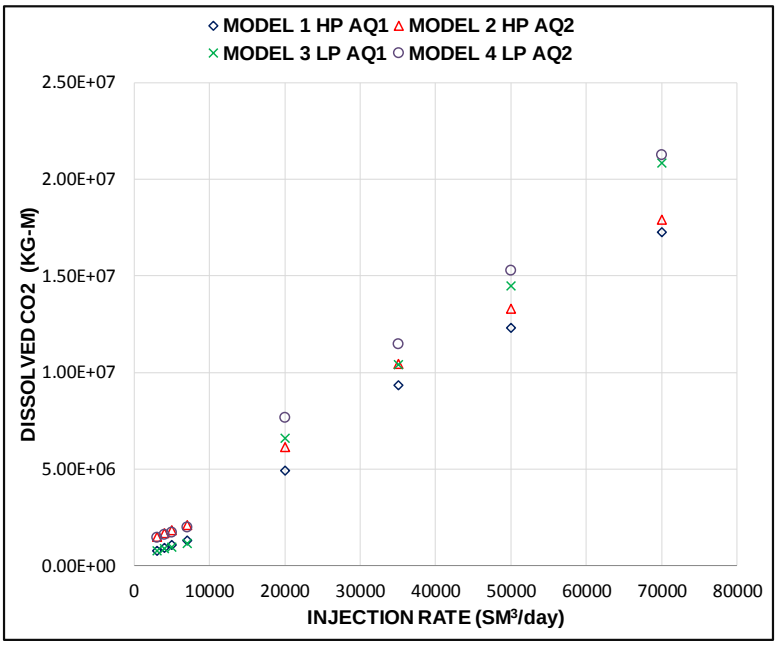


Fig.8 Amount of dissolved $CO_2$ at the end of the post injection period for all injection scenarios.

Figure 9 demonstrates the free gas saturation for a rather low injection rate of $5\times10^3$ $SM^3$/day in all four models. The least free gas is observed using Models 2 and 4 with the perforation at

the bottom of Aquifer 2, since more $CO_2$ was dissolved for these models because of the highest interaction between the brine and the $CO_2$. The highest amount of free gas is observed using Models 1 and 3 with less dissolved $CO_2$ in the water phase. Figure 10 shows the free gas saturation at a higher injection rate of $70\times10^3$ $SM^3$/day. The lowest free gas saturation is seen using Model 4, since more $CO_2$ was dissolved in this model as a result of the combined effects of the higher pressure and longer migration distance. Once the $CO_2$ dissolves in the water phase, it can no longer exist as a free gas. Therefore, it is not possible for the $CO_2$ to travel upwards under buoyancy; hence, the security and effectiveness of the storage will be improved.

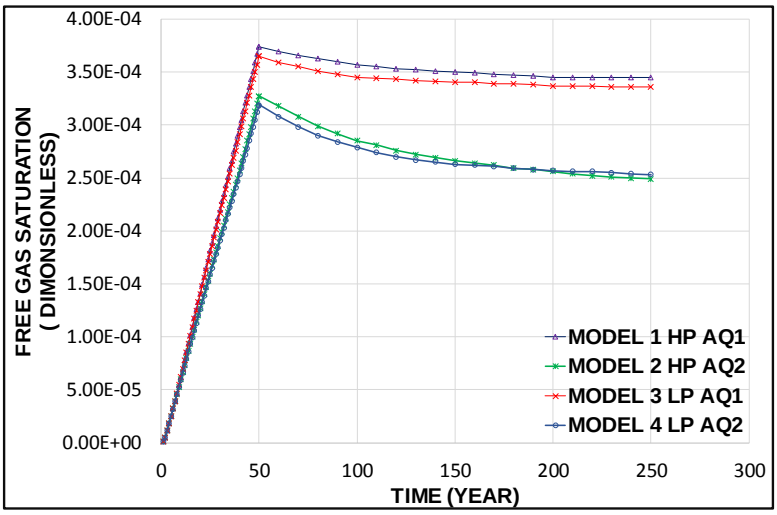


Fig.9 Free gas saturation (dimensionless) at $5\times10^3$ $SM^3$/day injection rate.

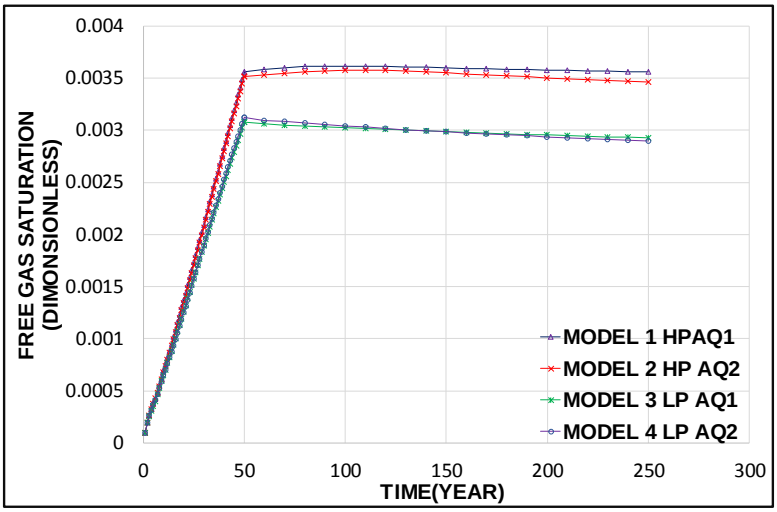


Fig.10 Free gas saturation (dimensionless) at $70\times10^3$ $SM^3$/day injection rate.

## 4. Effect of salinity and temperature gradient on $CO_2$ dissolution

The temperature of the subsurface formation depends on the geothermal gradient in that specific region. Temperature changes linearly by depth. Normally, the salinity of the formations water in sedimentary basins gradually increases by increasing the depth. In this part, the effects of constant reservoir temperature, temperature gradient, constant reservoir salinity and salinity gradient are investigated.

### 4.1 Temperature effect

In order to observe the effect of reservoir temperature on $CO_2$ dissolution, different temperature values were first assigned to the models ($31^oC$, $35^oC$, $40^oC$, $45^oC$, $50^oC$). In this step, the temperature gradient was not taken into consideration. As expected, the field of dissolved $CO_2$ in the water phase is seen to decrease as the temperature increases (Figure 11). By increasing temperature, the solubility of the $CO_2$ in brine decreases. Furthermore, the viscosity of the brine decreases as temperature increases. In the $CO_2$ and water displacement system, relative permeability, irreducible saturation and capillary pressure play important roles. These characteristics**,** along with other factors, rely on the interfacial tension between the formation water and the $CO_2$. In a situation when salinity and pressure are constant (similar to the research conditions), the interfacial tension between the $CO_2$ and the formation water increases with an increasing temperature (Bachu and Bennion 2009). Moreover, a generally inverse relationship exists between the interfacial tension of the $CO_2$ and the formation water and the solubility of $CO_2$ in the water phase.

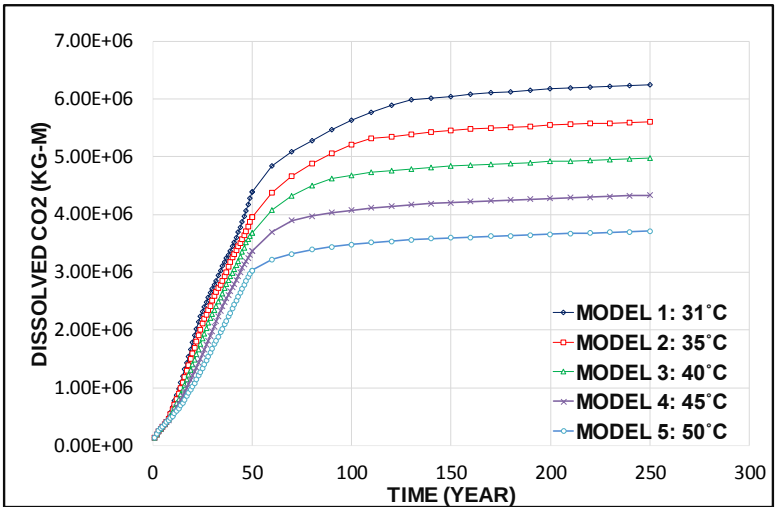


Fig.11 Effect of constant reservoir temperature on $CO_2$ dissolution.

### 4.1.1 Effect of temperature gradient on $CO_2$ dissolution

Two models were constructed in order to investigate the effects of the temperature gradient. The geothermal gradient was created by assigning different values of temperature to a different depth. For the temperature gradient of 2$^o$C/100m, at the datum depth, the temperature was assigned to be 33$^o$C. Then, the temperature was increased (2$^o$C/100m) linearly with the depth. For the temperature gradient of 5$^o$C/100m, at the datum depth, the temperature was assigned to be 60$^o$C. Again, the temperature was increased (5$^o$C/100m) linearly with the depth.

One of these models had a temperature gradient of 2$^o$C/100m, which is a cold basin, while the other model had a higher temperature gradient of 5$^o$C/100m, which is a warm basin. Figure 12 demonstrates the effects of the two different geothermal gradients on $CO_2$ dissolution.

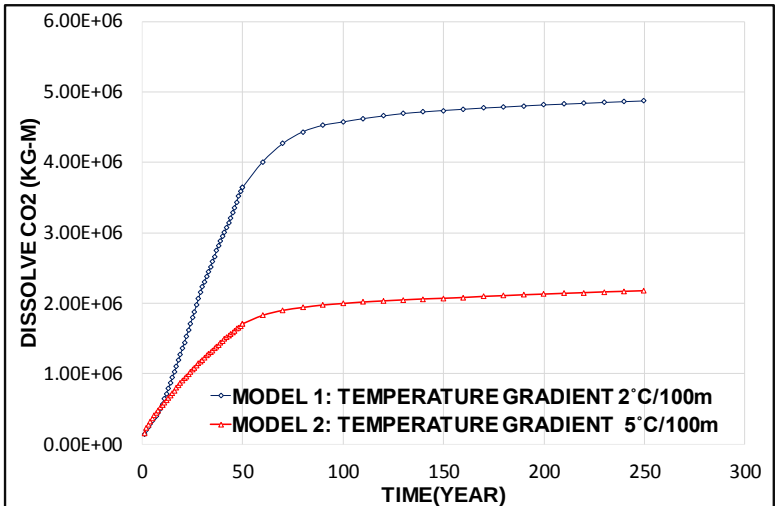


297 Fig.12 Effect of temperature gradient on $CO_2$ dissolution.

298 Obviously noticeable from this figure is that in the model with the higher temperature gradient
299 ($5^oC$), the field of dissolved $CO_2$ in the formation water drastically decreased. This is because
300 for higher temperature gradients, the solubility of $CO_2$ in the water phase is less than its
301 solubility in lower temperature gradients. In other words, brine in cooler basins can contain
302 more $CO_2$ than warmer ones. Furthermore, the difference in dissolved $CO_2$ in these two
303 gradients starts at the beginning of the injection period, since $CO_2$ was injected at the bottom
304 of the aquifer where the temperature have the highest value. This fact had a major influence on
305 the $CO_2$ dissolution from the start of the simulation.

306 At the end of the injection period, the amount of dissolved $CO_2$ in the water phase is 5.61E+06
307 Kg-m in the model with the constant reservoir temperature of $35^oC$. In the model with the
308 temperature gradient of $2^oC$/100m, the amount of dissolved $CO_2$ in the water phase is 4.87E+06
309 Kg-m indicating a significant decrease (12%) in $CO_2$ dissolution. Figure 13 demonstrates this
310 difference. Hence, ignoring the temperature gradient leads to overestimating the amount of
311 dissolved $CO_2$ in the aquifer and the storage capacity.

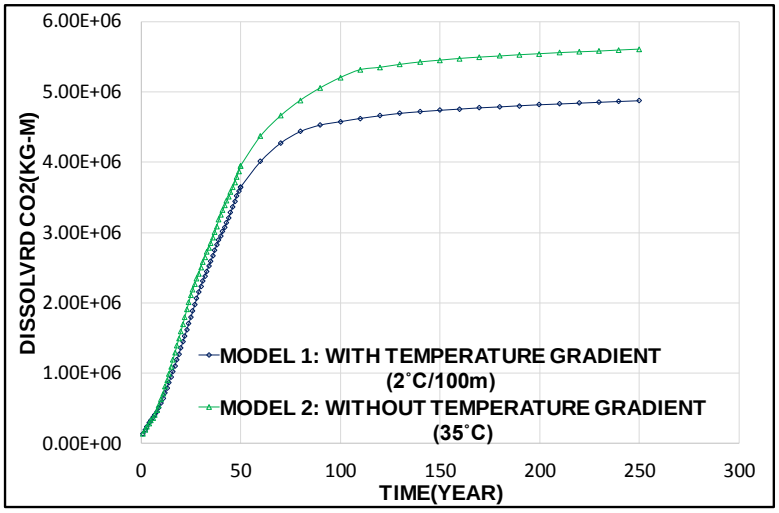


Fig.13 Comparison between Models with and without a temperature gradient.

## 4.2 Salinity effects

In order to examine the impacts of formation water salinity on $CO_2$ dissolution, five models with salinity levels of 10,000 mg/L, 75,000 mg/L, 100,000 mg/L, 165,000 mg/L, and 200,000 mg/L were generated. In these models, the reservoir temperature was assumed to be constant (35$^{o}$C).

As predicted, the amount of dissolved $CO_2$ in the aquifer decreases as the salinity increases (Figure 14). The brine density increases by increasing the salt concentration. Hence, due to the density difference between the formation water and the $CO_2$, the buoyancy forces play a more active role. Consequently, the interaction between the brine and the $CO_2$ is reduced. Therefore, the degree of the solubility trapping as a major trapping mechanism is dependent on salinity. By increasing brine salinity, the degree of solubility trapping is decreased (Johnson et al. 2004). In order to improve the effectiveness of this type of trapping mechanism and minimise the upward migration of $CO_2$ under buoyancy, the salinity of the formation water must be considered. Aquifers with low salinities are freshwater resources (<1000 mg/L) and need to be conserved. Thus, the salinity of the formation water needs to be moderate.

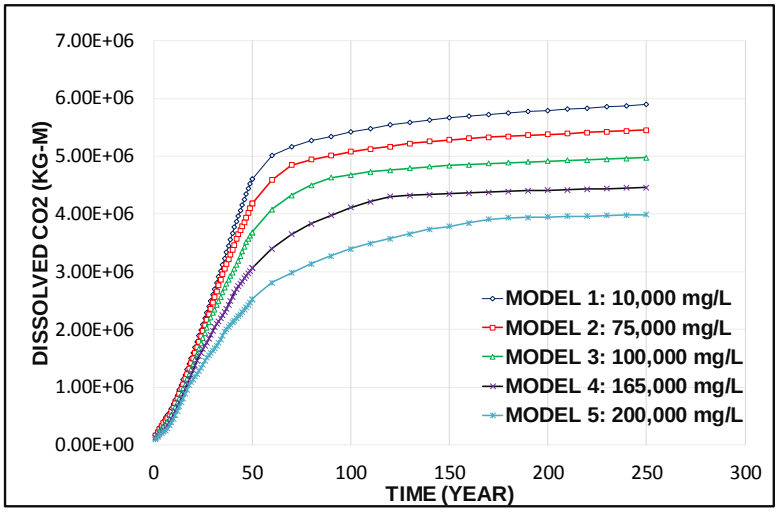


Fig.14 Effect of constant reservoir salinity on $CO_2$ dissolution.

### 4.2.1 Effect of salinity gradient on $CO_2$ dissolution

Dickey (1969) demonstrated that salinity changes with depth at a rate of 50 mg/L to 300 mg/L per m. The overall composition ($CO_2$, $H_2O$, and NaCl) of the formation was modified with depth to examine and evaluate the effect of the salinity gradient on the solubility of $CO_2$. The mole fraction at datum depth was 0.0, 0.967 and 0.033 for $CO_2$, $H_2O$ and NaCl respectively. For example, Model 1 had a salinity gradient of 120 mg/L/m. Therefore, the mole fractions of 0.0, 0.96 and 0.04 were assigned to the model at a depth of 1100. Model 2 used a salinity gradient of 250 mg/L/m. Therefore, the mole fractions of 0.0, 0.95 and 0.05 were assigned to the model at a depth of 1100. These models used a constant reservoir temperature of 35$^{o}$C.

Figure 15 demonstrates the effect of salinity gradient on $CO_2$ dissolution in the water phase. It is evident from this figure that the $CO_2$ dissolution in the water phase decreases by increasing the salinity of the formation water with depth.

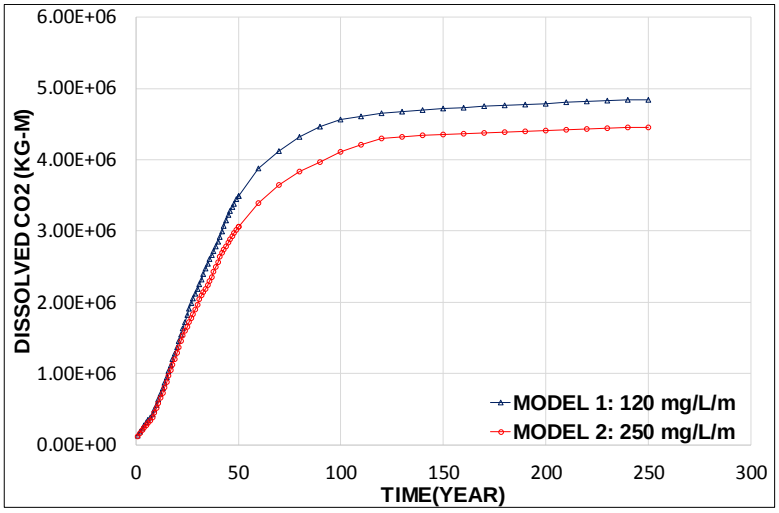


Fig.15 Effect of the salinity gradient on $CO_2$ dissolution.

At the end of the injection period, the amount of dissolved $CO_2$ in the water phase is 4.46E+06 Kg-m in the model with the constant reservoir salinity. The amount of dissolved $CO_2$ in the water phase is 4.67E+06 Kg-m in the model with the salinity gradient of 250 mg/L/m. Comparing the models with and without the salinity gradient, but at a close average salinity, demonstrates the difference (4%) and the importance of considering the salinity gradient for the amount of $CO_2$ dissolution. Figure 16 shows this comparison. Ignoring the salinity gradient leads to underestimating the amount of dissolved $CO_2$ in the aquifer.

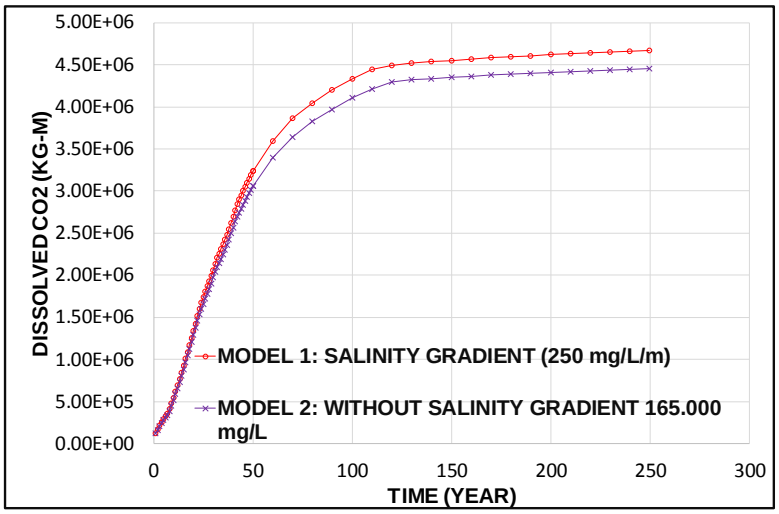


Fig.16 Comparison between Models with and without the salinity gradient.

## 5. The combined effect of salinity gradients, temperature gradients and injection rates on $CO_2$ dissolution

24 models were constructed in order to investigate the combined effects of salinity gradients, temperature gradients, and different injection scenarios, using two salinity gradients, two temperature gradients and six different injection rates. Figure 17 demonstrates the amount of dissolved $CO_2$ in the water phase in these 24 model simulations for the 200 years post-injection period. Models with low salinity and temperature gradients have the capacity to dissolve the most $CO_2$ and models with high salinity and temperature gradients have the capacity to dissolve the least. From this figure, it is clear that for lower $CO_2$ injection rates of $3\times10^3$, $4\times10^3$, $5\times10^3$ and $7\times10^3$ $SM^3$/day, the effects of salinity gradients and temperature gradients on $CO_2$ dissolution are almost negligible. However, at higher injection rates of $20\times10^3$ and $40\times10^3$ $SM^3$/day; this effect becomes noticeable. Higher injection rates trigger the models to be more sensitive to higher salinity and temperature gradients, due to the consequential pressure increase which is not the case in lower injection rates. In addition, for the low injection rates, the injected $CO_2$ does not reach those depths with substantially different temperature and salinity gradients. Therefore, the effect of variation in salinity and temperature on the amount of dissolved $CO_2$ is insignificant.

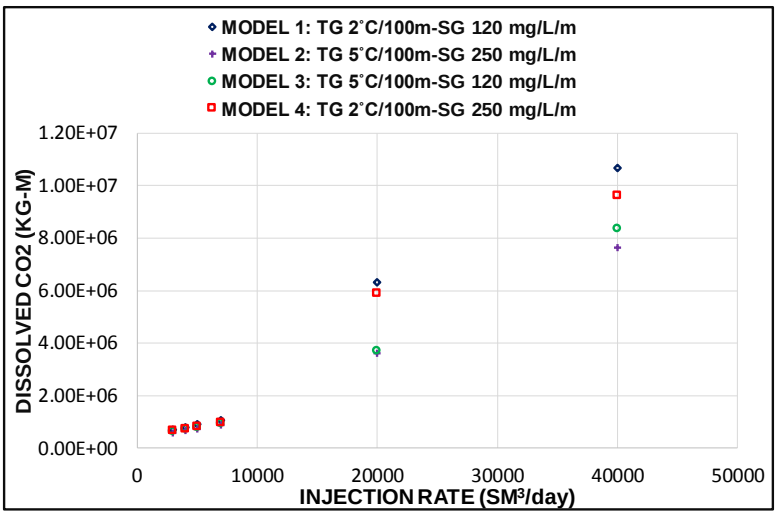


Fig.17 Amount of dissolved $CO_2$ in models with a different temperature gradient, salinity gradient and a different injection rate.

## 6. Conclusion

The main intention of $CO_2$ storage is to maximize the amount of $CO_2$ that can be injected into an aquifer and minimise the leakage potential as a mitigation option.

While investigating the unconformity surface as a type of aquifer and caprock interface on $CO_2$ dissolution it was observed:

1. When the injection rate is rather low, the distance travelled by the $CO_2$ plays a significant role towards increasing the total amount of $CO_2$ becoming dissolved. A longer distance means increased interaction between the brine and the $CO_2$ and therefore a higher dissolution in the water phase. When $CO_2$ is injected at the bottom of Aquifer 2, the amount of dissolved $CO_2$ is higher due to the greater distance to the top of the interval. Moreover, $CO_2$ dissolution in aquifers with a high-permeable conductive layer is higher than for aquifers without the high-permeable layer at lower injection rates. This layer provides a pathway to other storage formations. Hence, $CO_2$ travels a longer distance which results in a higher $CO_2$ dissolution.
2. When the injection rate is relatively high, dissolution is increased in closed aquifers with a low-permeable layer. The highest dissolved $CO_2$ is observed using the model with a low-permeable layer at an unconformity surface and when the $CO_2$ was injected at the bottom of Aquifer 2. This is due to the fact that for higher injection rates, the pressure builds up and more $CO_2$ will be dissolved in the water phase. Moreover, more dissolution occurs when the pathway to the caprock is longer, as the brine and $CO_2$ interaction is increased. Therefore, in the presence of a low-permeability layer, injection rates play a more effective role in $CO_2$ dissolution, as long as the pressure does not reach the pressure constraint.

3. Less free gas was also observed in the aquifers with the higher amount of $CO_2$ dissolution in the water phase. A higher amount of free $CO_2$ in the aquifers means a higher leakage potential and therefore a reduction of $CO_2$ storage security.
4. Overall, it is crucial to have precise injection rate and also the well and perforation location to maximise the storage potential and security of a $CO_2$ storage project.
5. $CO_2$ dissolution is affected by aquifer salinity and reservoir temperature. In warmer aquifers, less $CO_2$ will be dissolved into the water phase. This is also the case for aquifers with a higher salinity. As expected, the amount of $CO_2$ dissolved in the water phase is reduced with an increase in temperature and salinity. In summary, these results indicate that warmer aquifers and aquifers with high salinity have a lower capacity to dissolve $CO_2$. However, the decrease of solubility is more drastic for the model simulations using higher temperature gradients than in the models with salinity gradients. The low solubility of $CO_2$ in high-salinity brines and high-temperature formations leaves more $CO_2$ in the gas phase, which reduces storage security. In addition, since the difference in the amount of dissolved $CO_2$ between models with and without temperature and salinity gradients is significant, considering the temperature and salinity gradient is crucial when selecting a formation for $CO_2$ storage. Ignoring them may cause overestimating or underestimating the storage capacity.
6. One of the interesting results was that for a lower injection rate, the effect of salinity and temperature gradients on $CO_2$ dissolution is almost negligible. However, at higher injection rates, the models' sensitivity to temperature and salinity gradient is significant due to higher pressure and a longer migration distance.
7. In sum, it is essential to consider salinity and temperature gradients in modelling studies as they have large effects on the amount of dissolved $CO_2$ in the brine and hence the storage capacity and security.

Since $CO_2$ storage efficiencies are related to the size of the connected aquifers, the formation heterogeneity and the $CO_2$ injection strategy, conducting heterogeneous models to investigate its effects on $CO_2$ dissolution are recommended for future studies.

## References


1. Bachu, S. and Adams, J. (2003) 'Sequestration of $CO_2$ in Geological Media in Response to Climate Change: Capacity of Deep Saline Aquifers to Sequester $CO_2$ in Solution'. *Energy Conversion and Management* 44 (20), 3151-3175.
2. Bachu, S. and Bennion, D.B. (2008) 'Interfacial tension between $CO_2$, freshwater, and brine in the range of pressure from (2 to 27) MPa, temperature from (20 to 125)°C, and water salinity from (0 to 334 000) mg· L− 1'. *Journal of Chemical & Engineering Data*, *54*(3), 765-775.
3. Bachu, S., Gunter, W. and Perkins, E. (1993) 'Aquifer Disposal of $CO_2$: Hydrodynamic and Mineral Trapping'. *Energy Conversion and Management* 35 (4), 269-279.
4. Biddle, K. T. and Wielchowsky, C. C. (1994) 'Hydrocarbon Traps'. *Memoirs-American Association of Petroleum Geologists*, 219-219.
5. Cao, J., Zhang, Y., Hu, W., Yao, S., Wang, X., Zhang, Y. and Tang, Y. (2005) 'The Permian hybrid petroleum system in the northwest margin of the Junggar Basin, Northwest China. *Marine and Petroleum Geology,* 22(3), 331-349.
6. Davison, J., Freund, P. and Smith, A. (2001) 'Putting Carbon Back into the Ground'. *IEA Greenhouse Gas R&D Programme* 28.
7. Dickey, P.A. (1969) 'Increasing Concentration of subsurface brines with depth. *Chemical Geology*, *4*(1-2), 361-370.
8. Evans, T.R. and Coleman, N.C. (1974). 'North Sea geothermal gradients'. *Nature*, *247* (5435), 28-30.

9. Fengjun, N., Sitian, L., Hua, W., Xinong, X., Keqiang, W. and Meizhu, J. (2001) 'Lateral igration pathways of petroleum in the Zhu III sub-basin, Pearl River Mouth basin, South China Sea. *Marine and Petroleum Geology*, 18(5), 561-575.
10. Gao, X., Liu, L., Jiang, Z., Shang, X. and Liu, G. (2013) A Pre-Paleogene unconformity surface of the Sikeshu Sag, Junggar Basin: Lithological, geophysical and geochemical implications for the transportation of hydrocarbons. *Geoscience Frontiers, 4*(6), 779-786.
11. Goater, A.L., Bijeljic, B. and Blunt, M.J. (2013) 'Dipping open Aquifers—the effect of top-surface topography and heterogeneity on $CO_2$ storage efficiency. *International Journal of Greenhouse Gas Control*, 17, 318-331.
12. Harper, M.L. (1971) 'Approximate geothermal gradients in the North Sea basin. *Nature*, *230*(5291), 235-236.
13. Holloway, S. (2009) 'Storage capacity and containment issues for carbon dioxide capture and geological storage on the UK continental shelf. *Proceedings of the Institution of Mechanical Engineers, Part A: Journal of Power and Energy*, *223*(3), 239-248.
14. IPCC (2005) *IPCC Special Report on Carbon Dioxide Capture and Storage*. In: METZ, B., DAVIDSON, O., DE CONINCK H.C., LOOS, M., MEYER, L.A. (Eds.), Prepared by Working Group III of the Intergovernmental Panel on Climate Change. Cambridge University Press, Cambridge, UK/New York, NY, USA, 442.
15. Johnson, J.W., Nitao, J.J. and Knauss, K.G. (2004) 'Reactive transport modelling of $CO_2$ storage in saline aquifers to elucidate fundamental processes, trapping mechanisms and sequestration partitioning'. *Geological Society, London, Special Publications*, *233*(1), 107-128.

16. Koide, H., Takahashi, M., Tsukamoto, H. and Shindo, Y. (1995) 'Self-Trapping Mechanisms of Carbon Dioxide in the Aquifer Disposal'. *Energy Conversion and Management* 36 (6), 505-508.
17. Mousavi Nezhad, M., Javadi, A.A. and Abbasi, F. (2011) 'Stochastic finite element modelling of water flow in variably saturated heterogeneous soils. *International Journal for Numerical and Analytical Methods in Geomechanics*, *35*(12), 1389-1408.
18. Mousavi Nezhad, M., Javadi, A.A. and Rezania, M. (2011) 'Modeling of contaminant transport in soils considering the effects of micro-and macro-heterogeneity. *Journal of hydrology*, *404*(3-4), 332-338.
19. Nilsen, H.M., Syversveen, A.R., Lie, K.A., Tveranger, J. and Nordbotten, J.M. (2012) Impact of top-surface morphology on $CO_2$ storage capacity. *International Journal of Greenhouse Gas Control*, *11*, pp.221-235.
20. Nordbotten, J.M., Celia, M.A. and Bachu, S. (2005). 'Injection and storage of $CO_2$ in deep saline Aquifers: Analytical solution for $CO_2$ plume evolution during injection'. *Transport in Porous Media*, *58*(3), 339-360.
21. Oldenburg, C.M. (2007) 'Migration mechanisms and potential impacts of $CO_2$ leakage and seepage'. *Carbon Capture and Sequestration Integrating Technology, Monitoring, and Regulation*, 127-146.
22. Peacock, S.M. (1996) Thermal and petrologic structure of subduction zones'. *Subduction top to bottom*, 119-133.
23. Rogers, J.N., Kelley, J.T., Belknap, D.F., Gontz, A. and Barnhardt, W.A. (2006) 'Shallow-water pockmark formation in temperate estuaries: a consideration of origins in the western gulf of Maine with special focus on Belfast Bay. *Marine Geology*, *225*(1), 45-62.

24. Saemundsson, K., Axelsson, G. and Steingrímsson, B. (2009) 'Geothermal systems in global perspective'. *Short Course on Exploration for Geothermal Resources, UNU GTP*, 11.
25. Shariatipour, S. M., Pickup, G. E. and Mackay, E. J. (2016a) 'Simulations of $CO_2$ storage in aquifer models with top surface morphology and transition zones'. *International Journal of Greenhouse Gas Control*, 54, 117-128.
26. Shariatipour, S. M., Pickup, G. E. and Mackay, E. J. (2016b). 'Investigation of $CO_2$ torage in a saline formation with an angular unconformity at the caprock interface. *Petroleum Geoscience*, 22(2), 203-210.
27. Shariatipour, S.M., Pickup, G.E. and Mackay, E.J. (2014) 'The Effect of Aquifer/Caprock Interface on Geological Storage of $CO_2$'. *Energy Procedia*, *63*, 5544-5555.
28. Smith, M., Campbell, D., Mackay, E. and Polson, D., 2011. CO2 aquifer storage site evaluation and monitoring. *Heriot Watt University, Edinburgh, ISBN*, pp.978-0.
29. Song, H., Huang, G., Li, T., Zhang, Y. and Lou, Y. (2014) Analytical model of CO2 storage efficiency in saline aquifer with vertical heterogeneity'. *Journal of Natural Gas Science and Engineering*, *18*, 77-89.
30. Song, Z., Song, H., Cao, Y., Killough, J., Leung, J., Huang, G. and Gao, S. (2015) 'Numerical research on CO2 storage efficiency in saline aquifer with low-velocity non-Darcy flow'. *Journal of Natural Gas Science and Engineering*, *23*, 338-345.
31. Spycher, N., Pruess, K. and Ennis-King, J. (2003) '$CO_2$-$H_2O$ mixtures in the geological sequestration of $CO_2$. I. Assessment and calculation of mutual solubilities from 12 to 100 $^{o}$C and up to 600 bar'. *Geochimica et Cosmochimica Acta*, *67*(16), 3015-3031.
32. Stern, N.H. (2006) *The Economics of climate change: the Stern review*. Cambridge: Cambridge University Press.

33. Swierczek, M. (2012) *Role of unconformities in controlling clastic reservoir properties: insights from adopting a multidisciplinary approach* (Doctoral dissertation: Heriot-Watt University.